Charged Particle Environment for NGST: L2 Plasma Environment Statistics

Joseph I. Minow*[a], William C. Blackwell[a], Linda F. Neergaard[a], Steven W. Evans[b], Donna M. Hardage[c], and Jerry K. Owens[b]

[a]Sverdrup Technology, Inc., Marshall Space Flight Center Group, Huntsville, AL 35806
[b]ED44/Environments Group, NASA/Marshall Space Flight Center, Huntsville, AL 35812
[c]ED03/Engineering Technology Development Office, NASA/MSFC, Huntsville, AL 35812

Abstract

The plasma environment encountered by the Next Generation Space Telescope satellite in a halo orbit about L2 can include the Earth's magnetotail and magnetosheath in addition to the solar wind depending on the orbital radius chosen for the mission. Analysis of plasma environment impacts on the satellite requires knowledge of the average and extreme plasma characteristics to assess the magnitude of spacecraft charging and materials degradation expected for the mission lifetime. This report describes the analysis of plasma data from instruments onboard the IMP 8 and Geotail spacecraft used to produce the plasma database for the LRAD engineering-level phenomenology code developed to provide the NGST L2 environment definition.

Keywords: NGST, L2, plasma, environment, modeling, magnetosheath, solar wind, magnetotail

1. Introduction

The proposed orbit for the Next Generation Space Telescope (NGST) spacecraft is a halo orbit about the second Lagrange point, L2, approximately 236 Earth radii (Re) from the Earth in the anti-solar direction where the spacecraft will encounter the solar wind and the Earth's magnetosheath in addition to the deep tail regions of the magnetosphere (see Figure 1a). Deep tail plasma regimes are highly variable in both space and time. Assessment of the deep tail (X_{GSE} < -100 R_E) plasma conditions for possible impacts on the NGST spacecraft requires consideration of the variability in the orientation and dimensions of the plasma regimes as well as the statistics of plasma characteristic variations within each regime. Time scales for solar wind variations and magnetospheric response is on the order of tens of minutes, short compared to the typical six month period of a halo orbit. Much of the variability in the plasma environments encountered by the NGST spacecraft will therefore be the result of different plasma regimes moving past a spacecraft that may be treated as stationary relative to the dynamic variations in the orientation and dimension of the deep tail. Computation of particle flux within individual plasma regions and fluence for complete halo orbits in such a dynamic environment are aided by the development of a model to provide a framework for incorporating statistical variations in plasma parameters and fluctuations in magnetotail structure and position due to time dependent variations in the solar wind.

The L2 radiation model (LRAD), an engineering-level plasma phenomenology code, was developed to provide estimates of the L2 plasma environment for satellites in halo orbits about L2 [1]. This report provides an overview to the satellite records of solar wind, magnetosheath, and magnetotail plasma data and the analysis used to produce the statistics of the plasma environment for the NGST environment definition. Results from the analysis of the data pertinent to the LRAD code are discussed since the plasma data used to derive the statistics are incorporated into the database for the LRAD model. Finally, we present two examples of applications of the plasma analysis to spacecraft environment interactions—spacecraft charging and sputtering—to demonstrate impacts of the plasma environments on the design of the NGST satellite.

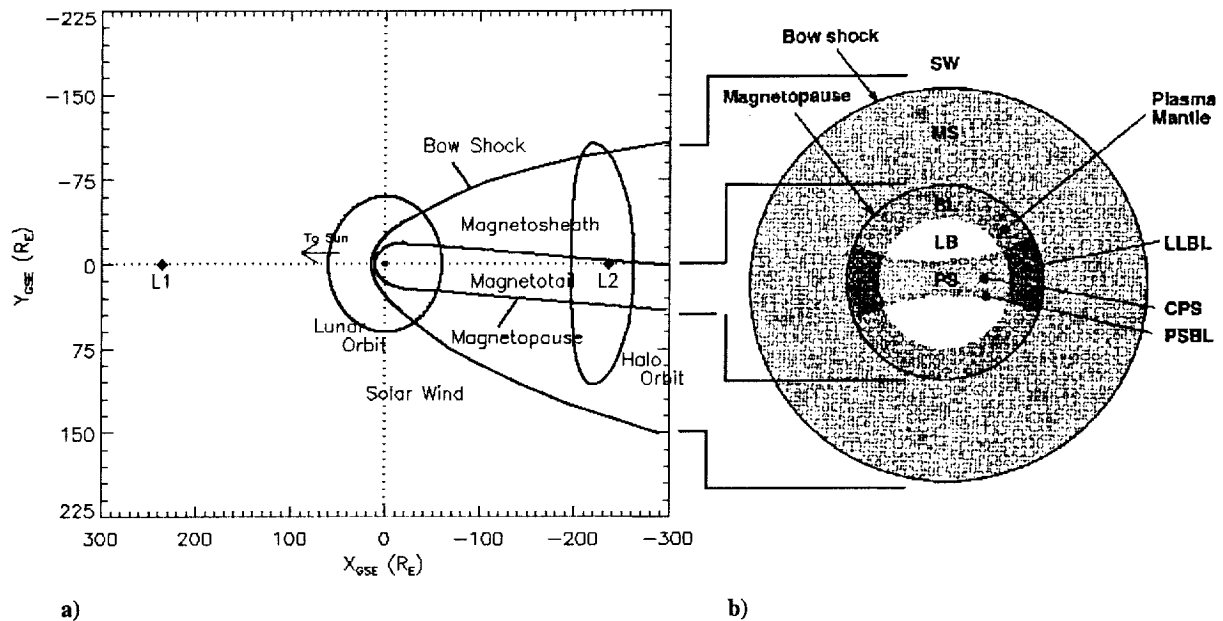*Correspondence: Email: joseph.minow@msfc.nasa.gov; Telephone: 256 544 2850; Fax: 256 544 0242

Figure 1. Magnetotail Plasma Environments. A schematic of the Earth-Moon system projected onto the ecliptic (GSE X-Y) plane showing the locations of the first and second Lagrange points, L1 and L2, relative to the Earth and lunar orbit. A sample halo orbit is indicated about L2 to demonstrate the magnitude of the orbital amplitudes relative to the dimensions of the magnetotail and magnetosheath at L2 distances. The cross section of the magnetotail in the GSE Y-Z plane indicates the magnetotail plasma regimes. Labels indicate the solar wind (SW), magnetosheath (MS), boundary layer (BL), lobe (LB), plasma sheet (PS), low latitude boundary layer (LLBL), central plasma sheet (CPS), and plasma sheet boundary layer (PSBL) (magnetotail plasma regime figure adapted from [2]).

2. Observations of Magnetotail Plasma Environments

The immense size of a typical L2 halo orbit relative to the dimensions of the magnetosphere is illustrated in Figure 1a. Satellites in a variety of halo orbits about L2 with different orbital amplitudes will spend an appreciable fraction of time in plasma regimes associated with the Earth's magnetosphere as well as the solar wind (c.f., [1]). Plasma regimes at deep tail distances fall into one of three main categories: the unperturbed solar wind, the magnetosheath, and the magnetotail. Spacecraft at downtail distances beyond approximately 50 R_E may be located in any of these plasma regimes at any time due to the tremendous variability in the dimension and orientation of the magnetotail at large distances from the Earth [1, 2].

A cross section in the Geocentric Solar Ecliptic (GSE) Y-Z plane illustrating the dominant plasma regimes identified over the years during satellite exploration of the magnetotail at various distances from the Earth is given in Figure 1b [2]. The solar wind, magnetosheath, boundary layer, lobe, and plasma sheet regions are clearly distinguishable in the deep tail although many of the subdivisions identified in the magnetotail nearer the Earth are not so apparent in plasma records obtained at L2 distances [2,3].

Relatively few spacecraft have sampled the plasma in the deep magnetotail. The two primary sources to date for deep tail plasma magnetic field records are the ISEE-3 mission during the late 1970's and early 1980's [4,5,6,7] and the more recent Geotail mission [2,3,8,9]. Geotail sampled the distant tail over a range of downtail distances from X_{GSE} = –50 Re to -209 Re over the period from late 1992 through the end of 1994.

Statistics for plasma regimes within the magnetotail and the magnetosheath incorporated into LRAD are obtained from records obtained by the University of Iowa Comprehensive Plasma Instrument (CPI) onboard the Geotail satellite. Plasma moments (number density, temperature, and flow velocities) from January through June 1993 were available for analysis. An example of this data is given in Figure 2 where all of the data from the six month period is plotted as a function of
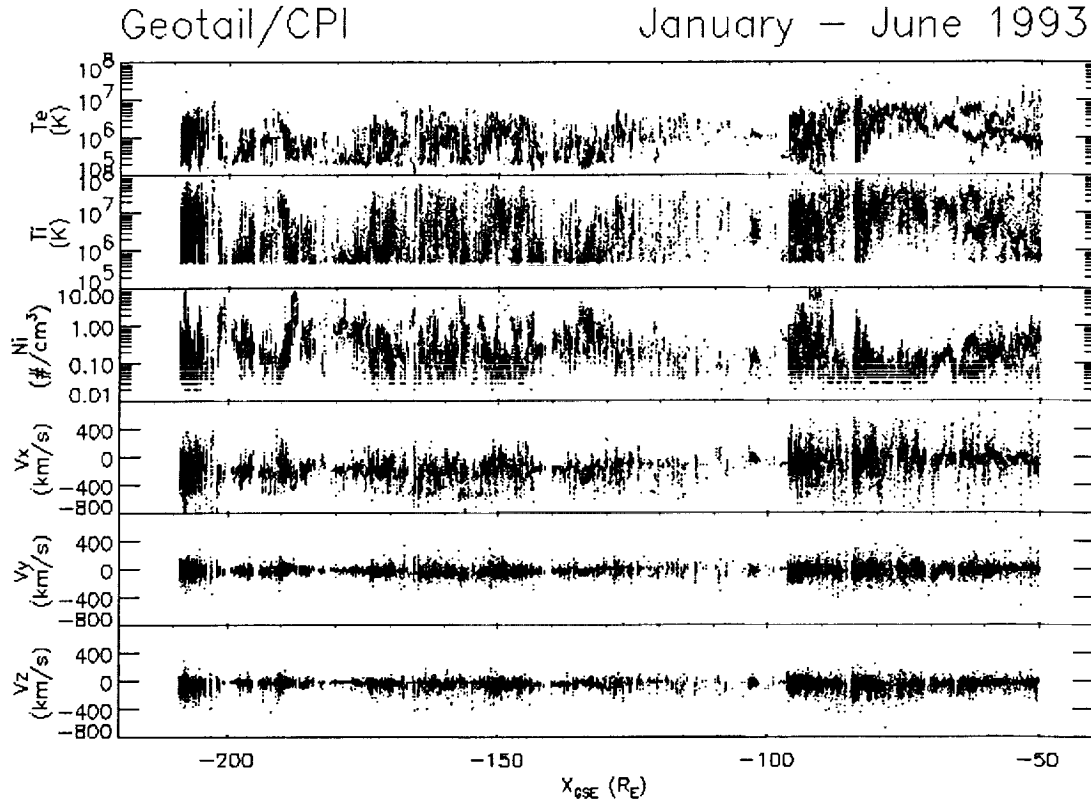
Figure 2. Survey of Magnetotail and Magnetosheath Plasma Characteristics. The data is from the University of Iowa/CPI instrument onboard the Geotail satellite for the first 180 days in 1993. Values for all GSE Y and Z distances are plotted on the same axis. Data gaps are due to the sparse sampling of deep tail plasma regimes during the four deep tail passes represented in the data set.

distance along the Sun-Earth line. Flow velocities and densities refer to the ions but both ion and electron temperatures were available in the data set. Four individual orbits through the deep tail are included in the data set providing samples of deep tail plasma environments over a range of distances from 50 R_E downstream of the Earth to a maximum distance of nearly 209 Re downstream of the Earth. Geotail plasma data is not available from L2 but the records shown in Figure 2 exhibit no significant trends in the plasma moments as a function of downtail distance for $X_{GSE} < -100$ Re. Previous studies of the magnetotail have shown that for $X_{GSE} < -50$ R_E the source of plasma encountered in the magnetotail is solar wind that entered the magnetosphere either through the dayside polar cusp or locally along the open magnetopause boundary. Magnetotail plasma beyond $X_{GSE} = -100$ R_E is nearly all due to solar wind entering the tail locally [10]. Deep tail plasma moments and composition therefore should exhibit similar characteristics for a wide range of distances in the magnetotail beyond approximately $X_{GSE} = -100$ R_E.

Identification of the plasma regimes for the Geotail CPI records is provided by the EPIC (Energetic Particle and Ion Composition instrument) Science Team [2,3]. The classification scheme uses the data from CPI in addition to a variety of other instruments onboard the Geotail spacecraft to classify the Geotail records as belonging to plasma sheet, lobe, boundary layer, magnetosheath, and solar wind plasma regimes. Adopting the EPIC Science Team plasma regime identifications facilitated the computation of the statistics for the electron and ion densities, velocities, and temperatures for each of the deep tail plasma regimes.

An alternative data source is required for information on the solar wind because solar wind encounters are not present in the Geotail data set shown in Figure 2. Solar wind properties presented here are from a number of the Interplanetary Monitoring Platform (IMP) satellites. The IMP series satellites were placed in near circular, 35 to 40 R_E orbits for observations of the solar wind and magnetosphere. Solar wind plasma characteristic statistics are obtained from data provided by the MIT Faraday Cup instrument onboard Interplanetary Monitoring Program (IMP) IMP-8 satellite. Data from an interval starting in
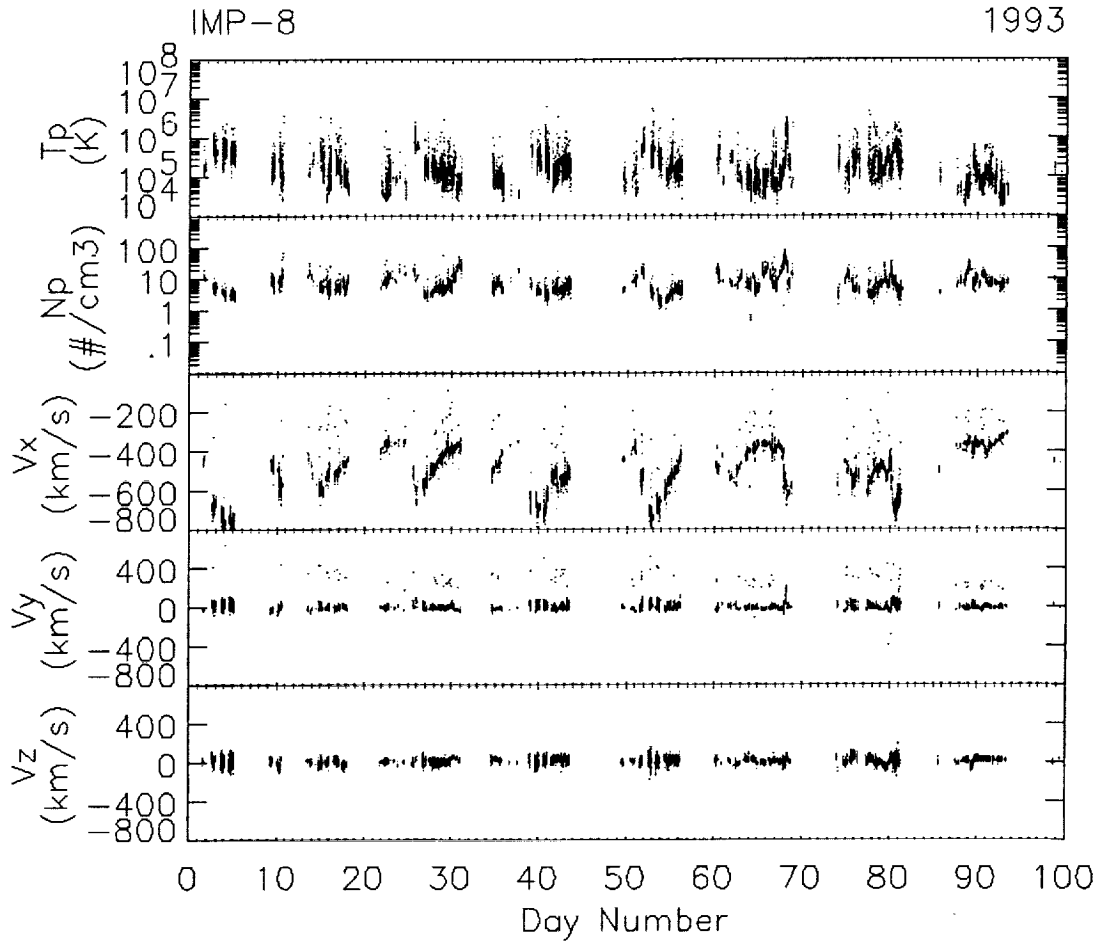
IMP-8   **1993**

Figure 3. Example 1993 IMP-8 Solar Wind Plasma Characteristics. The large data gaps in the data set occur when the satellite is inside the magnetosheath and magnetosphere. The dominant velocity component, Vx, although variable is always negative indicating the plasma environment in the solar wind is highly anisotropic.

early November 1973 through the end of December 1998 are included in the analysis, a time period spanning almost three complete solar cycles. A sample of IMP-8 records is shown in Figure 3.

Plasma populations in all regimes are quasi-neutral such that the electron and net ion densities are equal, a useful plasma property since electron densities are not available in the IMP-8 records. Electron densities are estimated from the quasi-neutral condition

$$N_e = \sum_k n_k N_k \tag{1}$$

where n_k is the charge state of the kth ion species of density N_k in a quasi-neutral plasma. It is generally sufficient to include only hydrogen and helium ions in the sum at L2 distances due to the relatively low abundance of heavy ions in the solar wind and distant magnetotail.

Electron and ion temperatures in the tables in the following sections are given in multiples of 1×10^4 K to facilitate conversion to electron volts (eV). Approximate temperatures in electron volts (with an error on the order of 20%) is read directly from the tables since the conversion between the units is 11604 K/1 eV.

Table 1. Radial Variations in Solar Wind Plasma Characteristics

Parameter	Radial Dependence	Reference
Plasma density	$n \propto R_S^{-2.1 \pm 0.3}$	[11]
Proton temperature	$T_p \propto R_S^{-0.57}$	[12]
Electron temperature	$Te \propto R_S^{-0.33}$	[12]
Magnetic field	$|\vec{B}| \propto 1/\sqrt{(R_S^{-2} + R_S^{-4})/2}$	[12]
Plasma velocity	Vsw = constant	[12]

3. Solar Wind Characteristics

Radial variations in plasma number density, temperature, and magnetic field intensity are given in Table 1 where R_S is the distance from the Sun to the Earth in Astronomical Units (AU). The scale length for variations in solar wind characteristics are sufficiently large that plasma data obtained from near the Earth are simply adopted for the L2 environment without correction for radial variations. Adding the 0.01 AU distance from Earth to L2 to the Sun-Earth distance of 1 AU yields L2 densities, temperatures, and magnetic fields less than a few percent different than values determined in the vicinity of the Earth. Formally the near Earth values should be corrected for the distance to L2 but the errors are small compared to the variations in each of the parameters. No correction is required for solar wind velocity since the magnitude of the flow speed is nearly constant between 1 and 20 AU [13].

3.1 Solar Wind Plasma Statistics

Table 2 contains statistics of solar wind plasma characteristics using data from the IMP 6, IMP 7 and IMP 8 satellites obtained over an interval from March 1971 through July 1974 [14]. Results from this study are included here because values for the electron, proton, and helium temperatures are available in addition to the ratio of helium to proton number densities. Table 3 contains results from an extended set of IMP 8 observations from 1973 through December 1998. The advantage of the latter data set, while only including proton observations, is the greater coverage over nearly three complete solar cycles in the time series to more completely explore range of variations in the proton density, temperature, and velocity.

Solar wind electrons are composed of two populations. A core population of high density, low energy electrons dominates with a minor density contribution due to a halo population of high temperature electrons. Density of the core population is typically ten times that of the halo population but only one tenth the temperature [13]. Two component plasma moments obtained from fits to a bi-Maxwellian velocity distribution is required to characterize both populations but this information is not available in the IMP 8 plasma moment records where numerical integrations of the velocity distribution were used to obtain the moments (c.f., [1]). The solar wind electron statistics presented here will therefore apply primarily to the dominant core population.

Species composition is shown in Table 4 for average solar wind, low speed solar wind, high speed solar wind, and a coronal mass ejection driver gas (a transient solar disturbance) are given as well to demonstrate the variability of ion composition for different solar wind conditions. Hydrogen ions dominate in all cases, with helium the most common minor species. Ions heavier than helium are present in the solar wind but represent a negligible contribution to the total solar wind mass. This same composition will also apply throughout the magnetosheath and into the magnetotail at L2 distances because the plasma source for the magnetotail beyond approximately 100 Re from the Earth is primarily the solar wind [10].

It should be noted that use of the values in Tables 1 through 3 are complicated by the requirement that correlations between the individual values must be considered to obtain meaningful results for extreme values of the electron and proton flux. For example, solar wind densities and speeds are generally anti-correlated, with the greatest densities occurring during periods of low speed flows and the smaller densities occurring in high speed solar wind flows. Examples of the anti-correlation are
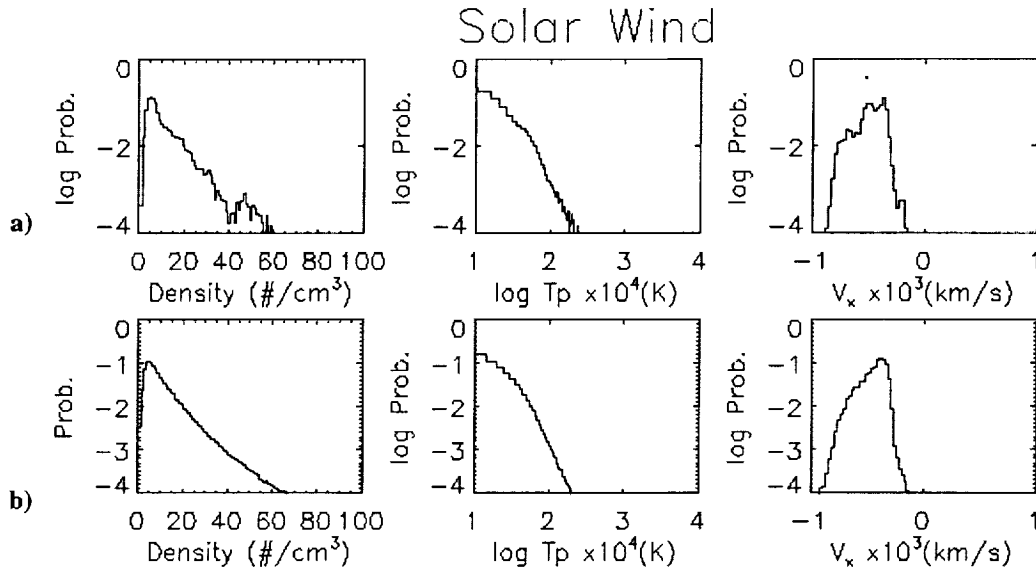
Figure 4. Statistics of Solar Wind Plasma Characteristics. (a) Histograms for data from January through June, 1993, corresponding to the Geotail plasma records shown in Figure 2. (b) Histograms for all records from November 1973 through December of 1998.

apparent in Figure 3 where the density is observed to decrease for large (negative) increases in solar wind velocity. The inverse relationship is described by [15]

$$N = C\ V^{-3/2} \tag{2}$$

where C is a constant of proportionality and V is the magnitude of the total solar wind flow velocity. The solar wind velocity and proton temperature, however, are correlated by [15]

$$T_p^{1/2} = A\ V + B \tag{3}$$

where the temperature is given in units of 1000K and the velocity in km/s. The constants A = 0.033 ± 0.0001 and B = -4.8± 0.4 have been found to be relatively constant over the period from 1966 through 1971, a significant fraction of a solar cycle [16]. Examples of the correlations are seen in Figure 3 where increases in the proton temperature accompany the increasingly large anti-solar plasma flow.

Histograms of the solar wind plasma are shown in Figure 4 to highlight the variations in the solar wind environment. Two sets of plots are included, the first in Figure 4a is only the first 6 months of 1993 which corresponds to the period the Geotail data was obtained for the magnetotail plasma regimes. Histograms in Figure 4b include the entire IMP 8 data set from November 1973 through the end of December 1998. The comparison has been included to demonstrate the double peak in the solar wind velocity that occurs in the six month subset from 1993. This same peak will appear in the Geotail velocity records to be described below and is the origin of the double peak in the flux and fluence statistics described by Blackwell et al. [1]. The double peak is most likely due to preferential sampling of plasma environments during a period of recurrent fast and low speed solar wind flows during the first half of 1993. Including data from a larger interval of time removes the double peak in the IMP 8 flow statistics and would likely do the same for the Geotail data if a larger data set could be obtained for the deep tail observations.

4. Magnetotail and Magnetosheath Plasma Analysis

Statistics for the magnetosheath and magnetotail plasma regimes from the Geotail CPI data are given in the form of histograms in Figure 5 and integrated probabilities in Table 4. Boundary layer and lobe records are lumped into a single set of histograms for Figure 5 since the boundary layers expand into the tail at great distances from the Earth and essentially fill the lobes with solar wind plasma at distances beyond X_{GSE} = -100 Re. The histograms demonstrate that plasma density in the

Table 1. Average Solar Wind Properties[a]

Parameter	Mean	σ	Most Probable	Median	5%-95% Limit		
N (#/cm^3)	8.7	6.6	5.0	6.9	3.0	to	20.0
V (km/s)	468	116	375	442	320	to	710
Tp x10^4(K)	12	9.1	5.0	9.5	0.98	to	30
Te x10^4(K)	14	3.9	12	13	8.9	to	20
Tα x10^4(K)	58	50	12	45	6.0	to	154
Nα/Np	0.047	0.019	0.048	0.047	0.017	to	0.078

[a]Adapted from [14]

Table 2. Statistics of IMP 8 Solar Wind Plasma Parameters[a]

Solar Wind Parameters (Protons Only)

Cum. Prob. (%)	Ni (#/cm3)	Vsw (km/s)	Tp x10^4(K)	Vx (km/s)	Vy (km/s)	Vz (km/s)
5	2.7	317.4	3.5	-649.4	-34.0	-31.3
33	5.4	380.3	9.0	-465.2	-13.1	2.9
50	7.2	414.6	13.5	-410.8	-4.5	17.2
67	9.8	469.4	20.5	-376.6	5.9	26.1
99	39.5	742.4	101.4	-290.4	78.1	85.7

[a]Based on analysis of November 1973 through December 1988
IMP 8 records.

Table 3. Solar Wind Ion Composition

Composition (relative to hydrogen)

Element	Average[a]	Low Speed[b]	High Speed[b]	CME Driver[b]
H	1.0	1.0	1.0	1.0
He	4.0×10^{-2}	0.04	0.04	>.15
O	5.2×10^{-4}	5.0×10^{-4}	8.0×10^{-4}	7.5×10^{-4}
Ne	7.5×10^{-5}	8.5×10^{-5}	---	---
Si	7.5×10^{-5}			
Ar	3.0×10^{-6}			
Fe	5.3×10^{-5}	5.0×10^{-5}	---	9.1×10^{-5}

[a]Adapted from [14]
[b]Adapted from [17]

magnetosheath is greater than in the magnetotail, while electron and ion temperatures are the greatest in the plasma sheet but are relatively low in the magnetosheath and boundary layers.

Although variable in magnitude, magnetosheath flow is always in the same anti-solar direction as the solar wind. The peak velocity in the lobe is less than in the magnetosheath but the majority of values are still in the anti-solar direction, consistent with a solar wind source of plasma for the boundary layers in the deep magnetotail. Plasma sheet velocities are biased towards anti-solar flow but a significant number of earthward flows are also present. Plasma fluxes in the deep tail will primarily impact the NGST spacecraft on the sunshield except in the plasma sheet where flows of a few hundred kilometers per second may occasionally drive plasma into the instrument side of the spacecraft. Finally, the origin of the double peaked velocity distribution in the magnetosheath and boundary layers was noted in the previous section.
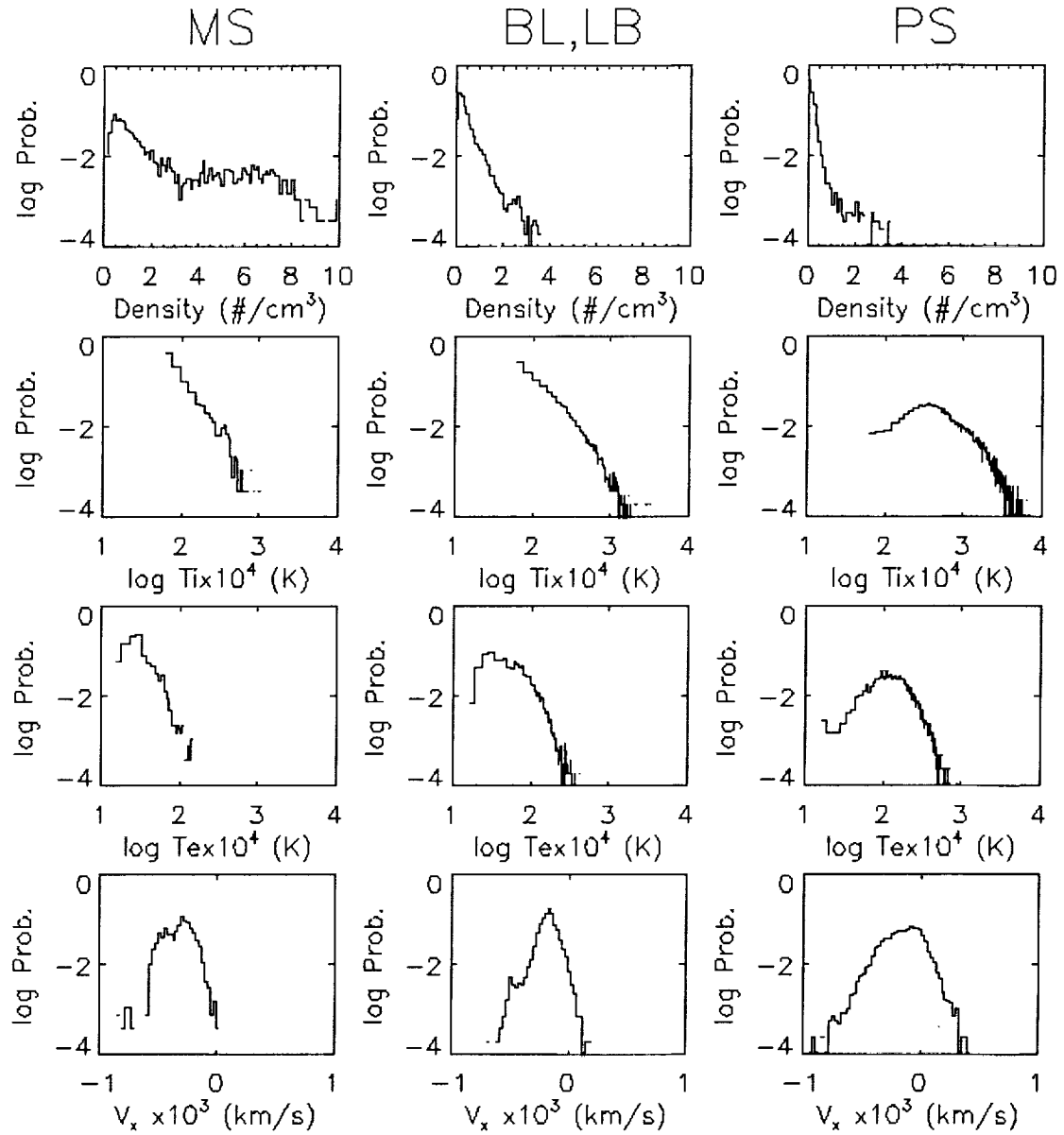
Figure 5. Magnetosheath and Magnetotail Plasma Characteristics. Histograms exhibit the mean as well as the variability range of values for each of the plasma characteristics.

Electron and helium characteristics not available in the solar wind and magnetotail plasma records are scaled in the current version of LRAD according to values in Table 4 based on a solar wind source for the plasma throughout the deep magnetotail.

Table 4. Plasma Parameter Scaling Factors

$$Tp = 5.5 \, Te$$
$$Talpha = Tp$$

Ne from the quasi-neutrality condition

$$Nalpha/Nproton = 0.047$$

Table 5. Statistical Variations in Magnetosheath and Magnetotail Plasma Parameters

Magnetosheath Parameters[a]

Cumulative Prob.	Ni (#/cc)	Ti x10^4(K)	Te x10^4(K)	Vx (km/s)	Vy (km/s)	Vz (km/s)
5	0.283	18.6	3.12	-519	-93.6	-52.3
33	0.687	75.5	20.6	-383	-50.0	-15.8
50	1.006	92.7	31.2	-311	-32.9	-7.21
67	1.645	110.	41.8	-272	-12.1	-0.88
99	8.684	461.	111.	-112	75.1	35.3

Boundary Layer Parameters[a]

Cumulative Prob.	Ni (#/cc)	Ti x104 (K)	Te x104 (K)	Vx (km/s)	Vy (km/s)	Vz (km/s)
5	0.108	30.9	6.03	-297.	-61.2	-68.8
33	0.235	90.3	39.8	-199.	-18.8	-23.6
50	0.316	114.	60.7	-167.	-5.67	-12.0
67	0.440	165.	84.9	-139.	6.87	-1.90
99	2.286	1220.	272.	2.49	74.4	58.7

Lobe Parameters[a]

Cumulative Prob.	Ni (#/cc)	Ti x104 (K)	Te x104 (K)	Vx (km/s)	Vy (km/s)	Vz (km/s)
5	0.010	93.7	75.2	-194.	-119.	-202.
33	0.069	405.	151.	-50.5	-23.0	-79.3
50	0.107	627.	205.	-24.0	5.62	-55.4
67	0.166	1180.	303.	11.5	33.6	-28.5
99	0.620	5880.	1650.	330.	208.	124.

Plasma Sheet Parameters[a]

Cumulative Prob.	Ni (#/cc)	Ti x104 (K)	Te x104 (K)	Vx (km/s)	Vy (km/s)	Vz (km/s)
5	0.015	185.	60.0	-378.	-104.	-148.
33	0.096	472.	130.	-134.	-25.4	-58.0
50	0.146	708.	169.	-62.0	-4.87	-36.0
67	0.196	1100.	228.	-10.1	14.7	-17.4
99	1.361	4740.	753.	308.	154.	81.0

[a]Based on analysis of Geotail Comprehensive Plasma Instrument records.
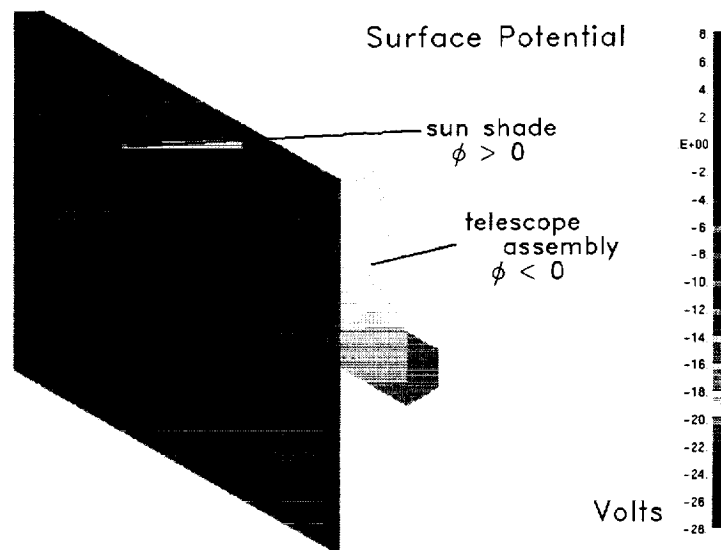
Figure 6. Example Charging Analysis. The hypothetical spacecraft shares many of the characteristics of the proposed NGST architectures. Orientation of the spacecraft is fixed with the sunshade illuminated by the sun and the instrument package/telescope structure in the shadow of the sunshade. The potential over most of the sunshade is positive while that of the instrument package/telescope structure charges to a negative potential.

5. Example of Plasma Effects

Spacecraft charging and surface degradation due to ion sputtering are two examples of plasma effects on a spacecraft. The origin of spacecraft charging differential collection of currents from the ambient plasma environment which balances the outgoing photoelectron, secondary electron, and secondary ion currents produced when charged particles collide with the spacecraft surface. Sputtering is a loss of atoms from the outer surface of the spacecraft primarily due to ion bombardment.

6.1 Spacecraft Charging

A simple order of magnitude estimate of the equilibrium potential expected for a spacecraft is obtained from the "rule of thumb" that a spacecraft structure in darkness will charge to a negative potential that is a few times the electron temperature since there is not outgoing photoelectron current to balance incident electron current from the ambient plasma environment [18]. Applying the "rule of thumb" to electron temperatures given in the tables above for a range of temperature of 50 eV to 200 eV suggest potentials on the order of −100 volts to -400 volts. Potentials as great as −1000 to -3000 volts are predicted using the "rule of thumb" in plasma regimes where the extreme electron temperatures may reach 500-1500 eV (c.f., the lobe and plasmsheet electron temperatures in Table 5).

The photoelectron currents leaving the sunlit surface of a spacecraft are typically much greater than the electron current to the surface from the plasma environment in the low density plasma regimes found outside of the Earth's inner magnetosphere. Illuminated spacecraft surfaces under these conditions will typically charge to positive potentials. Pederson et al. [19] obtained the empirical relationship

$$\Phi \text{ (volts)} = 9 Ne[cm^{-3}]^{-0.44} \tag{4}$$

for the spacecraft potential φ if the external plasma density is between 0.0001 cm^{-3} and 10 cm^{-3}. These simple scaling laws suggest the sunlit surface of the NGST sunshield will charge to potentials of approximately positive tens of volts. The greatest positive potentials are expected when the plasma density is the least, in the plasma sheet and lobes, and may reach values of 50-60 volts.

Output from a NASCAP GEO charging analysis in Figure 6 shows surface potentials for a candidate spacecraft with an architecture similar to that proposed for NGST. This model is not meant to suffice for a complete charging analysis for the NGST design since the exact material properties, spacecraft configurations, and the final orbit design for the mission have

Table 6. Solar Wind Environment for NASCAP GEO Calculation

Ambient Electrons	Ambient Ions (protons)
$Ne = 8.7 \ \#/cm^3$	$Np = 8.0 \ \#/cm^3$
$Te = 10 \ eV$	$Tp = 2.5 \ eV$

yet to be defined. We have simply adopted an architecture that places an instrument package in the shadow of a sunshade to demonstrate that a standard charging model confirms the predictions from the "rule of thumb" and scaling laws for the spacecraft surface potentials. The conditions used for the environment in the NASCAP calculation are listed in Table 9.

Although NASCAP GEO is known to underestimate surface potentials in sunlight due to a limited solar photon spectrum included in the model when used in low density plasma environments [I. Katz, *personal communication*, 2000], the results in Figure 6 are consistent with the simple scaling laws. Using the electron density value in Table 6, Equation 4 predicts a surface potential of approximately +3.5 volts for the surface of the illuminated sunshade while the NASCAP result in Figure 6 exhibits a potential between +6 and +8 volts over most of the sunshade surface. Applying the "rule of thumb" to the 10 eV electron temperature used in the NASCAP analysis predicts potentials of –20 to –30 for the telescope structure in darkness, consistent with the NASCAP result of -14 volts to –20 volts. A more sophisticated analysis of spacecraft charging will require material properties and details of the satellite architecture since conductivity of the surface materials and grounding of the various components is a major factor in determing the nature of the surface potentials.

6.2 Ion Sputtering

Ions will remove material from the spacecraft surface through an ablation process primarily in the solar wind and magnetosheath where the bulk flow velocity imparts energies to ions of a few keV. Ion sputtering has been shown to be an important process for removing contaminants on Langmiur probes in the solar wind [20] and may impact thin materials and coatings used in the construction of NGST. Light ion sputtering yields for 1 keV projectiles are typically 10^{-2} for hydrogen, 10^{-1} for helium, and 1 for oxygen on metals [21].

7. Summary

Plasma records from the IMP-8 and Geotail spacecraft have provided the basis of the database used in the LRAD deep tail plasma environment model. Statistics of the deep tail environment obtained from these records are useful in estimating plasma impacts on spacecraft to be placed in orbits about L2. Examples of plasma interactions with spacecraft surfaces showed that while not expected to be very serious to the NGST satellite, some areas of concern will require further analysis and laboratory testing to assure the reliable operation of the spacecraft.

Acknowledgements

References

1. Blackwell et al., Charged particle environment for NGST: Model development, this volume, 2000.
2. Eastman, T.E., Christon, S.P., T. Doke, L.A. Frank, G. Gloeckler, H. Kojima, S. Kokubun, A.T.Y. Lui, H. Matsumoto, R.W. McEntire, T. Mukai, S.R. Nylund, W.R. Paterson, E.C. Roelof, Y. Saito, T. Sotirelis, K. Tsuruda, D.J. Williams, and T. Yamamoto, Magnetospheric plasma regimes identified using Geotail meausrements 2. Regime identification and distant tail variability, *J. Geophys. Res.*, 103, 23521 – 23542, 1998.
3. Christon, S.P., T.E. Eastman, T. Doke, L.A. Frank, G. Gloeckler, H. Kojima, S. Kokubun, A.T.Y. Lui,

H. Matsumoto, R.W. McEntire, T. Mukai, S.R. Nylund, W.R. Paterson, E.C. Roelof, Y. Saito, T. Sotirelis, K. Tsuruda, D.J. Williams, and T. Yamamoto, Magnetospheric plasma regimes identified using Geotail measurements 2. Statistics, spatial distribution, and geomagnetic dependence, *J. Geophys. Res., 103, 23521 – 23542, 1998.*

4.   Bame, S.J., et. al., Plasma regimes in the deep geomagnetic tail: ISEE-3, Geophys. Res. Letters, 10, 912 – 915, 1983.

5.   Cowley, S.W.H., et al., Energetic ion regimes in the deep geomagnetic tail: ISEE-3, Geophys. Res. Lett., 11, 275 – 278, 1984.

6.   Fairfield, D.H., On the structure of the distant magnetotail: ISEE-3, J. Geophys. Res., 97, 1403 – 1410, 1992.

7.   Slavin, J.A., et al., An ISEE 3 study of average and substorm conditions in the distant magnetotail, J. Geophys. Res., 90, 10875 – 10895, 1985.

8.   Paterson, W.R., and L.A. Frank, Survey of plasma parameters in Earth's distant magnetotail with the Geotail spacecraft, Geophys. Res. Lett., 21, 2971 – 2974, 1994.

9.   Maezawa, K., and T. Hori, The distant magnetotail: Its structure, IMF dependence, and thermal properties, *in New Perspectives on the Earth's Magnetotail,* AGU Monograph 105, (ed. by A. Nishida, D.N. Baker, and S.W.H. Cowley), American Geophysical Union, Washington, D.C., pp. 1 – 19, 1998.

10. Baker, D.N., and T.I. Pulkinnen, Large-scale structure of the magnetosphere, *in New Perspectives on the Earth's Magnetotail,* AGU Monograph 105, (ed. by A. Nishida, D.N. Baker, and S.W.H. Cowley), American Geophysical Union, Washington, D.C., pp. 21 – 31, 1998

11. Belcher, J.W., A.J. Lazarus, R.L. McNutt, Jr., and G.S. Gordon, Solar wind conditions in the outer heliosphere and the distance to the termination shock, J. Geophys. Res., 98, 2177, 1993.

12. Smith, E.J., and A. Barnes, Spatial dependences in the distant solar wind: Pioneers 10 and 11, p. 521 in *NASA CP 2280, Solar Wind 5,* 1983.

13. Cravens, T.E., *Physics of Solar System Plasmas,* Cambridge University Press, Atmospheric and Space Science Series, 1997.

14. Feldman W.C., J.R. Asbridge, S.J. Bame, and J.T. Gosling, Plasma and Magnetic Fields from the Sun, in *The Solar Output and its Variation,* (ed.) Oran R. White, Colorado Associated University Press, Boulder, 1977.

15. Burlaga, L.F., and K.W. Ogilvie, Heating of the solar wind, *Astrophys. J.,* 159, 659, 1970.

16. Burlaga, L.F., and K.W. Ogilvie, Solar wind temperature and speed, *J. Geophys. Res.,* 78, 2028, 1973.

17   Geiss, J., and P. Bochsler, Solar wind composition and what we expect to learn from out-of-ecliptic measurements, in *The Sun and the Heliosphere in Three Dimensions,* pp. 173 – 186, (ed.) R.G. Marsden, D. Reidel Pub. Co., 1986.

18   Moore, T.E., C.J. Pollock, and D.T. Young, Kinetic Core Plasma Diagnostics, in *Measurement Techniques in Space Plasmas: Particles,* Geophysical Monograph 102, edited by R.B. Pfaff, J.E. Borovsky, and D.T. Young, pp. 105 – 123, American Geophysical Union, Washington, D.C., 1998.

19   Pederson, A., Solar wind and magnetospher plasma diagnostics by spacecraft electrostatic potential meausrements, *Ann. Geophys.,* 13, 118 – 129, 1995.

20   Brace, L.H., Langmuir probe measurements in the ionosphere, in *Measurement Techniques in Space Plasmas: Particles,* Geophysical Monograph 102, edited by R.B. Pfaff, J.E. Borovsky, and D.T. Young, pp. 23 – 35, American Geophysical Union, Washington, D.C., 1998.

21. Behrisch, R., (ed.), *Sputtering by Particle Bombardment I, Physical Sputtering of Single-Element Solids,* Topics in Applied Physics, Volume 47, Springer-Verlag, 1981.